ESAIM: M2AN 54 (2020) 957–976
https://doi.org/10.1051/m2an/2019091

ESAIM: Mathematical Modelling and Numerical Analysis
www.esaim-m2an.org

LOCALIZATION AND GEOMETRIZATION IN PLASMON RESONANCES AND GEOMETRIC STRUCTURES OF NEUMANN-POINCARÉ EIGENFUNCTIONS

Emilia Blåsten[1], Hongjie Li[2], Hongyu Liu[3,*] and Yuliang Wang[4]

Abstract. This paper reports some interesting discoveries about the localization and geometrization phenomenon in plasmon resonances and the intrinsic geometric structures of Neumann-Poincaré eigenfunctions. It is known that plasmon resonance generically occurs in the quasi-static regime where the size of the plasmonic inclusion is sufficiently small compared to the wavelength. In this paper, we show that the global smallness condition on the plasmonic inclusion can be replaced by a local high-curvature condition, and the plasmon resonance occurs locally near the high-curvature point of the plasmonic inclusion. We link this phenomenon with the geometric structures of the Neumann-Poincaré (NP) eigenfunctions. The spectrum of the Neumann-Poincaré operator has received significant attentions in the literature. We show that the Neumann-Poincaré eigenfunctions possess some intrinsic geometric structures near the high-curvature points. We mainly rely on numerics to present our findings. For a particular case when the domain is an ellipse, we can provide the analytic results based on the explicit solutions.

Mathematics Subject Classification. 35Q60, 47G40, 35B30, 35R30.

Received May 7, 2019. Accepted December 13, 2019.

1. Introduction

There is considerable interest in the mathematical study of plasmon materials in recent years. Plasmon materials are a type of metamaterials that are artificially engineered to allow the presence of negative material parameters. We refer to [3, 5, 9, 23], [1, 2, 6, 13–15, 25, 30, 33–36, 38–44] and [7, 8, 10, 11, 16, 17, 24, 26–28, 31] and the references therein for the relevant studies in acoustics, electromagnetism and elasticity, respectively.

One peculiar and intriguing phenomenon associated with the plasmon materials is the so-called anomalous resonance [35]. Mathematically, the plasmon resonance is associated to the infinite dimensional kernel of a certain non-elliptic partial differential operator (PDO). In fact, the presence of negative material parameters breaks the ellipticity of the underlying partial differential equations (PDEs) that govern the various physical phenomena. Consequently, the non-elliptic PDO may possess a nontrivial kernel, which in turn may induce various resonance phenomena due to appropriate external excitations. In Ammari *et al.* [1], applying techniques

Keywords and phrases. Plasmonics, localization, geometrization, high-curvature, Neumann-Poincaré eigenfunctions.

[1] Department of Mathematics, University of Helsinki, Helsinki, Finland.
[2] Department of Mathematics, The Chinese University of Hong Kong, Shatin, Hong Kong SAR, PR China.
[3] Department of Mathematics, City University of Hong Kong, Kowloon, Hong Kong SAR, PR China.
[4] Department of Mathematics, Hong Kong Baptist University, Kowloon, Hong Kong SAR, PR China.
*Corresponding author: hongyu.liuip@gmail.com, hongyliu@cityu.edu.hk

from the layer potential theory, the plasmon resonance is connected to the spectrum of the classical Neumann-Poincaré (NP) operator. Indeed, the aforementioned nontrivial kernel function of the underlying non-elliptic PDO can be represented as a single-layer potential. In order for plasmon resonance to occur, the density function of the above single-layer potential has to be an eigenfunction of the corresponding Neumann-Poincaré operator. In such a way, the plasmon parameters are also connected to the eigenvalues of the corresponding NP operator in a delicate way. The spectral properties of the NP operator were recently extensively investigated in the literature [10, 16, 19–22, 29]. However, the corresponding studies are mainly concerned with the spectra of various NP operators in different geometric or physical setups. In this paper, we discover certain intrinsic geometric structures of the NP eigenfunctions. In fact, it is shown that the NP eigenfunctions as well as the associated single-layer potentials possess certain curvature-dependent behaviours locally near a boundary point. The geometric results can be used to provide theoretical explanation of the localization and geometrization phenomenon in plasmon resonances, which is another novel and intriguing discovery in this paper, and also one of the major motivations for the investigation of the geometric structures of NP eigenfunctions. It is emphasized that we mainly rely on numerics to present our findings. For a particular case when the domain is an ellipse, we can provide the analytic results based on the explicit solutions.

The localization and geometrization in wave scattering were proposed in Blåsten and Liu [12]. It states that if a certain wave scattering phenomenon occurs associated with a small object compared to the wavelength, then the similar phenomenon occurs for a "big" object but locally near a high-curvature boundary point. Noting that the global smallness condition means that the curvature is intrinsically high everywhere and hence the introduction of a local high-curvature condition is a natural one for the occurrence of the local scattering behaviour. In Blåsten and Liu [12], the localization and geometrization phenomena were shown and justified in several time-harmonic scattering scenarios. In this paper, we show that the same principle actually holds for the plasmon resonances. In fact, in many of the existing studies on plasmon resonances, the quasi-static approximation has played a critical role where the plasmonic inclusion is of a size much smaller than the wavelength. There are also several studies that go beyond the quasi-static limit [23, 29, 32, 35]. In Milton and Nicorovici [35], double negative materials are employed in the shell. In Kettunen *et al.* [23], it is actually shown that resonance does not occur for the classical core-shell plasmonic structure without the quasistatic approximation as long as the core and shell are strictly convex. In Li and Liu [29], Li *et al.* [32], in order for the plasmon resonances to occur beyond the quasi-static approximation, the corresponding plasmonic configuration has to be designed in a subtle and delicate way. Nevertheless, we show that for a plasmonic structure that is resonant in the quasi-static regime but non-resonant out of the quasi-static regime, the resonance always occurs locally near a high-curvature boundary point of the plasmonic inclusion. That is, the localization and geometrization phenomenon occurs for the plasmon resonances. This is mainly demonstrated by certain generic numerical examples. To seek a theoretical explanation, it naturally leads to the investigation of the geometric properties of the NP eigenfunctions as well as the associated single-layer potentials near a high-curvature boundary point.

The focus of our study is to present the interesting discoveries on the localization and geometrization in plasmon resonances as well as the intrinsic geometric structures of the NP eigenfunctions. We present our results mainly for the two-dimensional case based on extensive numerical experiments though the extension to the three-dimensional case as well as the rigorous theoretical justifications are also appealing for further study.

The rest of the paper is organized as follows. In Sections 2 and 3, we briefly discuss the plasmon resonances in the electrostatic and quasi-static cases. Section 4 presents the localization and geometrization phenomenon in the plasmon resonances. In Section 5, we investigate the geometric structures of the NP eigenfunctions. The paper is concluded in Section 6 with some relevant discussions.

2. Plasmon resonance in electrostatics and spectral system of NP operator

Let D be a bounded domain in $\mathbb{R}^2$ with a C^2-smooth boundary ∂D and a connected complement $\mathbb{R}^2\backslash\overline{D}$. Consider a dielectric medium configuration as follows,

$$\epsilon_\delta(x) = \begin{cases} \epsilon_c + i\delta, & x \in D, \\ 1, & x \in \mathbb{R}^2\backslash\overline{D}, \end{cases} \tag{2.1}$$

where $\epsilon_c \in \mathbb{R}_-$ and $\delta \in \mathbb{R}_+$. Let $u \in H^1_{\mathrm{loc}}(\mathbb{R}^2)$ signify the electric field associated with the medium configuration (2.1), and it satisfies the following PDE system,

$$\begin{cases} \nabla \cdot (\epsilon_\delta(x)\nabla u_\delta(x)) = f(x), & x \in \mathbb{R}^2, \\ u(x) = \mathcal{O}\left(\dfrac{1}{|x|}\right) & \text{as } |x| \to \infty, \end{cases} \tag{2.2}$$

where $f \in L^2(\mathbb{R}^2)$ is compactly supported in $\mathbb{R}^2\backslash\overline{D}$ and

$$\int_{\mathbb{R}^2} f(x)\, dx = 0.$$

Associated with the electrostatic system (2.2), the configuration (ϵ_δ, f) is said to be *resonant* if there holds

$$\mathbf{E}_\delta(\epsilon_\delta, f) := \frac{\delta}{2}\int_D |\nabla u_\delta|^2 \, \mathrm{d}x \to \infty \quad \text{as} \quad \delta \to +0. \tag{2.3}$$

The condition (2.3) indicates that if plasmon resonance occurs, then highly oscillating behaviours are exhibited by the resonant field around the plasmon inclusion. Mathematically, the resonance is induced by the nontrivial kernel of the non-elliptic PDO (partial differential operator)

$$L_{\epsilon_0} u := \nabla \cdot (\epsilon_0 \nabla u), \tag{2.4}$$

where ϵ_0 is ϵ_δ with δ formally taken to be zero. The kernel of L_{ϵ_0} consists of nontrivial functions satisfying

$$u \in H^1_{\mathrm{loc}}(\mathbb{R}^2); \quad L_{\epsilon_0} u(x) = 0, \quad x \in \mathbb{R}^2; \quad u(x) = \mathcal{O}\left(\frac{1}{|x|}\right) \text{ as } |x| \to \infty. \tag{2.5}$$

It is noted that ϵ_c is allowed to be negative, and hence the PDO L_{ϵ_0} is a non-elliptic operator. Therefore, if the plasmon constant ϵ_c is properly chosen, $\mathrm{Ker}(L_{\epsilon_0})$ as defined in (2.5) can be nonempty, which in turn can induce resonance as described in (2.3) for a properly chosen external source f.

The connection to the spectral system of the Neumann-Poincaré operator can be described as follows. By the layer-potential theory, one seeks a solution to (2.5) of the following form

$$u(x) = S_{\partial D}[\varphi](x), \quad \varphi \in L^2_0(\partial D), \tag{2.6}$$

where $L^2_0(\partial D)$ is the space of square integrable functions with zero average on ∂D, and $S_{\partial D}[\varphi]$ is the singe-layer operator defined as

$$S_{\partial D}[\varphi](x) := \int_{\partial D} G(x-y)\varphi(y)\mathrm{d}s(y), \quad x \in \mathbb{R}^2, \tag{2.7}$$

with

$$G(x) = \frac{1}{2\pi}\ln|x|, \tag{2.8}$$

being the fundamental solution of the Laplace operator in two dimensions. On the boundary ∂D, the single layer potential enjoys the following jump relationship

$$\partial_\nu S_{\partial D}[\varphi]|_\pm(x) = \left(\pm\frac{1}{2} + K^*_{\partial D}\right)[\varphi](x), \quad x \in \partial D, \tag{2.9}$$

where ∂_ν is the outward unit normal to ∂D and $\pm$ indicate the limits to ∂D from outside and inside of D, respectively. In (2.9), the operator $K^*_{\partial D}$ is defined as

$$K^*_{\partial D}[\varphi](x) = \frac{1}{2\pi}\int_{\partial D} \frac{\langle x-y, \nu_x\rangle}{|x-y|^2}\varphi(y)\mathrm{d}s(y), \quad x \in \partial D, \tag{2.10}$$

which is called the Neumann-Poincaré (NP) operator. By matching the transmission conditions across the boundary,

$$u|_- = u|_+, \quad \epsilon_c \partial_\nu u|_- = \partial_\nu u|_+, \tag{2.11}$$

and with the help of the jump formula (2.9), solving the system (2.5) is equivalent to solving the following problem

$$K^*_{\partial D}[\varphi](x) = \frac{\epsilon_c + 1}{2(\epsilon_c - 1)}\varphi(x), \quad x \in \partial D. \tag{2.12}$$

Clearly, according to our discussion made above, for the occurrence of the plasmon resonances, there are two critical conditions to be fulfilled from a spectral perspective associated with the NP operator defined in (2.10). First, the plasmon constant ϵ_c should be properly chosen such that the parameter $\lambda(\epsilon_c)$ defined as

$$\lambda(\epsilon_c) = \frac{\epsilon_c + 1}{2(\epsilon_c - 1)}, \tag{2.13}$$

belong to the spectrum of the NP operator K^*. Second, the single layer potential given in (2.6) associated with the NP eigenfunction φ according to (2.12) should exhibit certain highly oscillating behaviours around the plasmonic inclusion. The second condition naturally leads to the investigation of the structures of the NP eigenfunctions.

3. Plasmon resonance for small inclusions: quasi-static approximation

In this section we consider the plasmon resonance for the wave scattering in the quasi-static regime. That is, the size of the plasmonic inclusion is much smaller than the underlying wavelength. To that end, we let Ω be a bounded domain in $\mathbb{R}^2$ with a C^2-smooth boundary $\partial\Omega$ and a connected complement $\mathbb{R}^2\backslash\overline{\Omega}$. Set $D = s\Omega$, where $s \in \mathbb{R}_+$ signifies a scaling parameter. Introduce the following plasmonic configuration,

$$\epsilon_{\mathcal{D},\delta}(x) = \begin{cases} \epsilon_c + i\delta, & x \in \mathcal{D}, \\ 1, & x \in \mathbb{R}^2\backslash\overline{\mathcal{D}}, \end{cases} \tag{3.1}$$

where $\mathcal{D} = D$ or Ω. Associated with the medium configuration (3.1) in D, the wave scattering is governed by the following Helmholtz system

$$\begin{cases} \nabla\cdot(\epsilon_{D,\delta}(x)\nabla u_\delta(x)) + k^2 u_\delta(x) = f(x), & x \in \mathbb{R}^2, \\ \lim\limits_{|x|\to\infty} |x|^{1/2}\left(\dfrac{x}{|x|}\cdot\nabla u_\delta - iku_\delta\right) \to 0 \ \text{ as } \ |x| \to \infty, \end{cases} \tag{3.2}$$

where $k \in \mathbb{R}_+$ signifies a wavenumber and $f(x)$ is an external source that is compactly supported in $\mathbb{R}^2\backslash\overline{D}$. The last limit in (3.2) is referred to as the Sommerfeld radiation condition. (3.2) describes the transverse electromagnetic wave scattering (cf. [4, 29]).

Similar to the electrostatic case, if (2.3) occurs for the wave field in (3.2), the configuration is said to be resonant. In order to study the plasmon resonance associated with the Helmholtz system (3.2), by a straightforward scaling argument, the PDE system (3.2) can be transformed to

$$\nabla \cdot (\epsilon_{\Omega,\delta}(x)\nabla v_\delta(x)) + s^2k^2 v_\delta(x) = \tilde{f}(x), \quad x \in \mathbb{R}^2, \tag{3.3}$$

where $v_\delta(x) = u_\delta(x/s)$ and $\tilde{f}(x) = f(x/s)$. In what follows, we introduce the following PDO,

$$(L_{\epsilon_{\Omega,0}} + s^2k^2)u := \nabla \cdot (\epsilon_{\Omega,0}\nabla u) + s^2k^2 u. \tag{3.4}$$

Similar to our discussion in the previous section, for the occurrence of the plasmon resonance, one needs to determine a nontrivial kernel of $L_{\epsilon_{\Omega,0}} + s^2k^2$ associated with a proper choice of ϵ_c. To that end, we introduce

$$S^k_{\partial D}[\varphi](x) := \int_{\partial D} G^k(x-y)\varphi(y)\mathrm{d}s(y), \quad x \in \mathbb{R}^2, \tag{3.5}$$

$$(K^k_{\partial D})^*[\varphi](x) := \int_{\partial D} \partial_{\nu_x} G^k(x-y)\varphi(y)\mathrm{d}s(y), \quad x \in \partial D, \tag{3.6}$$

where

$$G^k(x) = -\frac{i}{4}H^1_0(k|x|),$$

with $H^1_0(t)$ zeroth-order Hankel function of the first kind. $S^k_{\partial D}$ and $(K^k_{\partial D})^*$ are, respectively, the single-layer potential and the NP operator with a finite frequency $k \in \mathbb{R}_+$ (cf. [4]). According to our earlier discussion in Section 2, in order to study the plasmon resonance associated with (3.1), it suffices to investigate the nontrivial kernel of the PDO $L_{\epsilon_{\Omega,0}} + s^2k^2$. Similar to the electrostatic case, by using the layer-potential techniques, the study is reduced to analyzing the spectral system of the NP operator $(K^{sk}_{\partial\Omega})^*$ and the highly oscillating behaviours of the single-layer potentials $S^{sk}_{\partial\Omega}[\varphi]$ with φ being the NP eigenfunctions. Imposing the quasi-static condition,

$$s \cdot k \ll 1, \tag{3.7}$$

one has that

$$-\frac{i}{4}H^1_0(sk|x|) = \frac{1}{2\pi}\ln|x| + \tau + \sum_{n=1}^{\infty}(b_n \ln(sk|x|) + c_n)(sk|x|)^{2n}, \tag{3.8}$$

where

$$\begin{aligned} b_n &= \frac{(-1)^n}{2\pi}\frac{1}{2^{2n}(n!)^2}, \quad c_n = -b_n\left(\gamma - \ln 2 - \frac{\pi i}{2} - \sum_{j=1}^{n}\frac{1}{j}\right), \\ \tau &= \frac{1}{2\pi}(\ln(sk) + \gamma - \ln 2) - \frac{i}{4}, \end{aligned} \tag{3.9}$$

with γ the Euler constant. Therefore one can derive the following asymptotic expansions

$$S^{sk}_{\partial\Omega} = S_{\partial\Omega} + \tau\langle\cdot, 1\rangle + (sk)^2\ln(sk)\mathcal{R}^{sk}, \tag{3.10}$$

where $\mathcal{R}^{sk}$ is a bounded operator from $L^2(\partial D)$ to $H^1(\partial D)$ and

$$(K^{sk}_{\partial\Omega})^* = K^*_{\partial\Omega} + (sk)^2\ln(sk)\mathcal{Q}^{sk}, \tag{3.11}$$

where the operator $\mathcal{Q}^{sk}$ is a bounded operator from $L^2(\partial\Omega)$ to itself. Hence, under the quasi-static approximation (3.7), the plasmon resonance for the Helmholtz system (3.2) again relies on the spectral properties of the NP

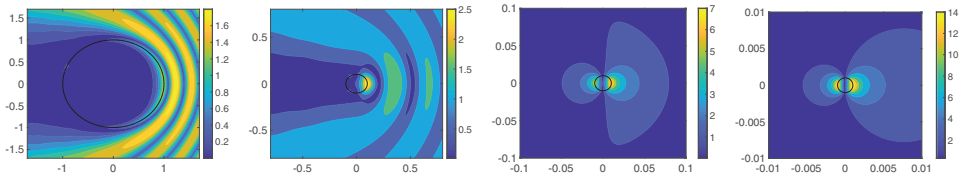

(a) (b) (c) (d)

FIGURE 1. Moduli of the total wave fields of (3.2), (3.13) and (3.14) with (a) $s = 2$; (b) $s = 0.2$; (c) $s = 0.02$; (d) $s = 0.002$.

operator $K^*_{\partial\Omega}$ and the oscillating behaviours of the corresponding single-layer potentials that are same to the electrostatic case. In fact, it is rigorously justified in [5,9] that under (3.7) and

$$s^2|\ln s|\delta^{-1} \ll 1, \tag{3.12}$$

the Helmholtz system (3.2) is resonant for ϵ_c chosen from the resonant electrostatic case (cf. [4]). Instead of discussing more theoretical details about the plasmon resonance within the quasi-static approximation, we next present several numerical examples for demonstration.

Consider a plasmon configuration of the form $\epsilon_{D,\delta}$ in (3.1) with

$$D = B_s(0), \quad \epsilon_c = -1, \quad \delta = 0.001, \tag{3.13}$$

where $B_s(0)$ is a central disc of radius $s \in \mathbb{R}_+$. The choice of $\epsilon_c = -1$ makes $\lambda(\epsilon_c)$ defined in (2.13) identically zero. It is noted that if D is a central disk, then 0 is actually the eigenvalue of K^*_D, and on the other hand, if D is an arbitrary domain with a C^2 boundary, K^*_D is a compact operator and 0 is an accumulation point of its eigenvalues. Hence, with $\epsilon_c = -1$, the first condition for the occurrence of the plasmon resonance is fulfilled. For the corresponding Helmholtz system (3.2), we choose

$$f = -\nabla\cdot(\epsilon_{D,\delta}\nabla u^i) - k^2u^i, \quad u^i(x) = e^{ikx\cdot d},\ k = 10,\ d = (-1,0). \tag{3.14}$$

That means, the wave scattering is caused by an incident plane wave which plays the role of an external source. In Figure 1, we plot the moduli of the total wave fields, namely $|u_\delta + u^i|$, against different parameters $s = 2$, $s = 0.2$, $s = 0.02$ and $s = 0.002$. The numerical results clearly show the critical role of the quasi-static approximation for the occurrence of the plasmon resonance. In fact, it can be seen that if the size of the plasmonic inclusion, namely $D = B_s(0)$, is not small enough compared to the wavelength, then resonance does not occur, and as s becomes smaller, both conditions (3.7) and (3.12) are fulfilled, then resonance occurs.

4. Localization and geometrization in plasmon resonance

In this section, we consider the localization and geometrization for the plasmon resonance. We first present some numerical examples to illustrate this kind of peculiar phenomenon. Our numerical examples follow a similar setup as that specified in (3.13) and (3.14) with $s = 2$. According to our study in the previous section, we know that resonance does not occur. However, we pull out a part of the boundary of the plasmonic inclusion D to form a boundary point with a relatively high curvature; see Figure 2 for the geometric setup. Similar to the numerical experiments in Figure 1, we numerically plot the total wave field associated to the plasmon inclusion as described above against the change of the curvature of the aforesaid boundary point; see Figure 3. It can be readily seen that as the curvature of that boundary point increases to a certain degree, then resonance occurs locally around that high-curvature point. This is referred to as the localization and geometrization in the plasmon resonance. By localization, we mean that the resonance occurs only locally around a boundary

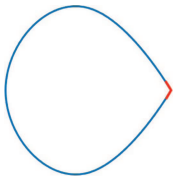

FIGURE 2. Geometry of the plasmonic inclusion D with a high-curvature boundary point.

point, whereas by geometrization, we mean that the global geometric smallness condition (3.7) can be replaced by a locally high-curvature condition. At this point, we would like to present our novel viewpoint about the plasmon resonance. That is, on the one hand, the plasmonic parameter is unquestionably a critical ingredient for the occurrence of resonance, but on the other hand, the quasi-static approximation, namely the smallness of the size of the plasmonic inclusion, is not the main cause for the resonance and instead, the high curvature is actually the main cause.

Next we try to provide a theoretical explanation of the localization and geometrization phenomenon in the plasmon resonance. According to our earlier discussion on the plasmon resonances, respectively, in the electrostatic and quasi-static cases, one needs to study the quantitative properties of the eigenfunctions of the NP operator $(K^k_{\partial D})^*$ in (3.6) and the corresponding single-layer potential $S^k_{\partial D}[\varphi]$ in (3.5) locally around the high-curvature point of ∂D. To that end, let us consider a domain D as plotted in Figure 2 and x_R be the vertex of the red part which possesses the largest curvature among all the boundary points. Set

$$\Gamma_1 := \partial D \cap B_\rho(x_R), \quad \Gamma_2 := \partial D \backslash \Gamma_1, \tag{4.1}$$

where $\rho \in \mathbb{R}_+$ is sufficiently small. We have

Proposition 4.1. *Let ∂D, Γ_1 and Γ_2 be described above. There holds*

$$\big(K^k_{\partial D}\big)^*\big|_{\Gamma_1} = K^*_{\Gamma_1} + \mathcal{R}_{\Gamma_1,\rho} + \mathcal{T}, \tag{4.2}$$

where $\mathcal{T}$ is a smooth operator on $L^2(\Gamma_1)$, and $\mathcal{R}_{\Gamma_1,\rho}$ is a bounded operator on $L^2(\Gamma_1)$ satisfying $\|\mathcal{R}_{\Gamma_1,\rho}\| = \mathcal{O}\big((\rho k)^2 \ln(\rho k)\big)$.

Proof. From (4.1), one has that

$$\big(K^k_{\partial D}\big)^*\big|_{\Gamma_1} = \big(K^k_{\Gamma_1}\big)^*\big|_{\Gamma_1} + \big(K^k_{\Gamma_2}\big)^*\big|_{\Gamma_1},$$

where $\big(K^k_{\Gamma_2}\big)^*\big|_{\Gamma_1}$ is smooth operator on $L^2(\Gamma_1)$. Since $\Gamma_1 := \partial D \cap B_\rho(x_R)$ with $\rho \in \mathbb{R}_+$ sufficiently small, from the asymptotic expression for the NP operator in (3.11), one has by direct calculations that

$$\big(K^k_{\Gamma_1}\big)^*\big|_{\Gamma_1} = K^*_{\Gamma_1}|_{\Gamma_1} + \mathcal{R}_{\Gamma_1,\rho},$$

where $\mathcal{R}_{\Gamma_1,\rho}$ is a bounded operator on $L^2(\Gamma_1)$ satisfying

$$\|\mathcal{R}_{\Gamma_1,\rho}\| = \mathcal{O}\big((\rho k)^2 \ln(\rho k)\big).$$

The proof is complete. □

Hence, by Proposition 4.1 and our earlier discussion on the plasmon resonance in the electrostatic and quasi-static cases, in order to understand the localization and geometrization phenomenon illustrated in Figure 3, it is unobjectionable to say that one should investigate the spectral properties of the eigenfunctions of $K^*_{\partial D}$ locally near a high-curvature point. The rest of the paper is devoted to investigating the geometric structures

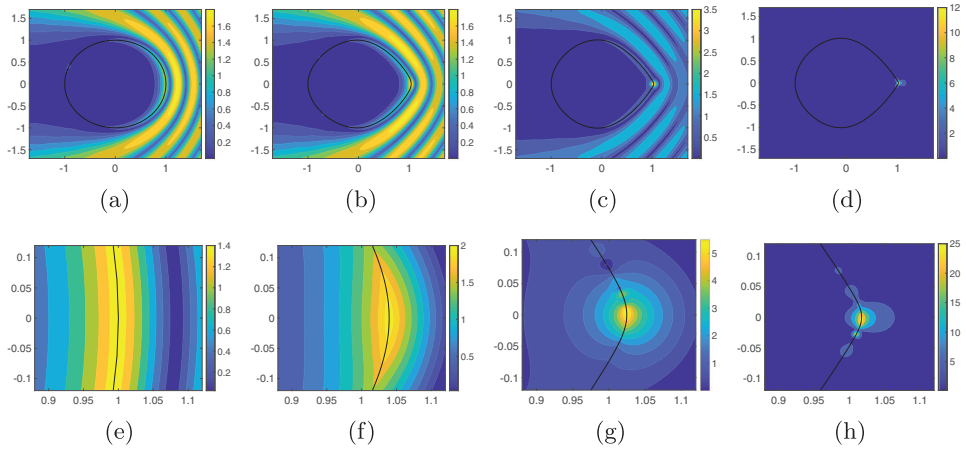

FIGURE 3. Localization and geometrization phenomenon in the plasmon resonance. The first row plots the moduli of the total fields with increasing curvatures at the same boundary point. The second row plots the moduli of the total fields locally around the high-curvature point.

of the NP eigenfunctions as well as the associated single-layer potentials near a high-curvature point. Finally, we mention that the geometrization with a high-curvature condition is a critical ingredient in our study. It is known that if ∂D is C^2-smooth, then the corresponding NP operator is compact, and hence its spectrum consists only of eigenvalues. If the high-curvature point becomes a corner, then the corresponding NP operator possesses continuous spectra [19, 22], which shall make the situation more complicated. Nevertheless, the NP operator may still possess eigenvalues in the corner domain case, and it is worth of future investigation on the corresponding NP eigenfunctions in such a case.

5. Geometric structures of NP eigenfunctions

In this section, we consider the geometric structures of the eigenfunctions of the NP operator $K^*_{\partial D}$ as well as the corresponding single layer potential $S_{\partial D}[\varphi]$ near a high-curvature point of ∂D.

First, we present some basic results about the spectral structure of $K^*_{\partial D}$. Throughout the rest of the paper, we assume that ∂D is C^2-smooth. As discussed earlier, $K^*_{\partial D}$ is a compact operator and its spectrum consists of at most countably many eigenvalues that can only accumulate at 0. We also know that (cf. [1])

$$\sigma(K^*_{\partial D}) \subset (-1/2, 1/2], \tag{5.1}$$

where and also in what follows, $\sigma(K^*_{\partial D})$ signifies the spectrum of $K^*_{\partial D}$. There holds the following property

Lemma 5.1. *Suppose that $\lambda_0 = 1/2$ is an eigenvalue of $K^*_{\partial D}$ and $\psi_0 \in L^2(\partial D)$ is an eigenfunction, i.e. $K^*_{\partial D}[\psi_0] = 1/2\psi_0$. Then there holds*

$$S_{\partial D}[\psi_0](x) = C \in \mathbb{C}, \quad x \in D.$$

Proof. The proof can be found in [4] and for a convenient reference, we present it in the following. Set

$$u(x) = S_{\partial D}[\psi_0](x), \quad x \in \mathbb{R}^2.$$

By Green's formula one can show that

$$\int_D |\nabla u|^2 \mathrm{d}x = \int_{\partial D} \frac{\partial u}{\partial \nu}\Big|_- \overline{u} \mathrm{d}s = \int_{\partial D} (K^*[\psi_0] - 1/2\psi_0)\, \overline{u} \mathrm{d}s = 0,$$

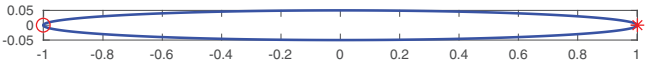

FIGURE 4. An ellipse defined by (5.2) and (5.4) with $R_0 = 1$ and $\rho_0 = 0.05$. The left and right vertices $x_\circ$ and x_*, respectively, on the semi-major axis are the high-curvature points.

where ν signifies the exterior unit normal vector to ∂D. Hence, u must be constant on ∂D.

The proof is complete. □

It is known that both $K^*_{\partial D}$ and $S_{\partial D}$ are pseudo-differential operators of order -1 (cf. [37]). Hence, if $\psi \in L^2(\partial D)$ is an eigenfunction satisfying $K^*_{\partial D}[\psi] = \lambda\psi$ for an eigenvalue $\lambda \in (-1/2, 1/2]$, it can be straightforwardly verify that $\psi \in C^{0,1}(\partial D)$. In fact, if ∂D is C^∞-smooth, then $\psi \in C^\infty(\partial D)$.

Next, we investigate the geometric structures of the NP eigenfunctions. We start with the case that ∂D is an ellipse whose NP eigenfunctions can be explicitly calculated. For $x = (x_1, x_2) \in \mathbb{R}^2$, we introduce the following elliptic coordinates (ρ, ω),

$$x_1 = R_0 \cos\omega \cosh\rho, \quad x_2 = R_0 \sin\omega \sinh\rho, \quad \rho > 0,\ 0 \le \omega \le 2\pi,\ R_0 \in \mathbb{R}_+. \tag{5.2}$$

An elliptic domain D is defined by

$$D = \{(\rho, \omega); \rho \le \rho_0,\ 0 \le \omega \le 2\pi\}, \tag{5.3}$$

whose boundary is given by

$$\partial D = \{(\rho, \omega); \rho = \rho_0,\ 0 \le \omega \le 2\pi\}. \tag{5.4}$$

In Figure 4 we give a specific example with $R_0 = 1$ and $\rho_0 = 0.05$. In what follows, we set

$$\Xi := R_0\sqrt{\sinh^2\rho_0 + \sin^2\omega}.$$

We have

Lemma 5.2 ([15]). *Let ∂D be an ellipse described in (5.2) and (5.4). There hold that*

$$K^*_{\partial D}[\phi_{1,n}] = a_n\phi_{1,n} \quad \text{and} \quad K^*_{\partial D}[\phi_{2,n}] = -a_n\phi_{2,n}, \quad n \ge 0,$$

where

$$\phi_{1,n} = \Xi^{-1}\cos n\omega, \quad \phi_{2,n} = \Xi^{-1}\sin n\omega \quad \text{and} \quad a_n = \frac{1}{2e^{2n\rho_0}}. \tag{5.5}$$

Moreover, associated with the eigenfunctions in (5.5), one has for $n \ge 1$ that

$$S_{\partial D}[\phi_{1,n}](x) = \begin{cases} -\frac{e^{n\rho}+e^{-n\rho}}{2ne^{n\rho_0}}\cos n\omega, & \rho \le \rho_0, \\ -\frac{e^{n\rho_0}+e^{-n\rho_0}}{2ne^{n\rho}}\cos n\omega, & \rho > \rho_0, \end{cases}$$

and

$$S_{\partial D}[\phi_{2,n}](x) = \begin{cases} -\frac{e^{n\rho}+e^{-n\rho}}{2ne^{n\rho_0}}\sin n\omega, & \rho \le \rho_0, \\ -\frac{e^{n\rho_0}+e^{-n\rho_0}}{2ne^{n\rho}}\sin n\omega, & \rho > \rho_0. \end{cases}$$

With the explicit forms of the NP eigenfunctions and the associated single-layer potentials, we are in a position to investigate their geometric structures. Before that, we first note that for an ellipse defined by (5.2) and (5.4), the corresponding curvature at a boundary point $(\rho_0, \omega) \in \partial D$ can be directly calculated to be

$$\kappa(\omega) = \frac{\cosh\rho_0 \sinh\rho_0}{R_0(\sinh^2\rho_0 + \sin^2\omega)^{3/2}}. \tag{5.6}$$

Hence, the largest curvature is attainable at the two vertices with $\omega = \pi$ and $\omega = 0$ respectively on the semi-major axis, denoted as $x_\circ$ and x_* in what follows; see Figure 4 for an illustration. Henceforth, the points on ∂D that attain the largest curvature are referred to as the high-curvature points. By (5.6), the largest curvature is given by

$$\kappa_{\max} := \frac{\cosh \rho_0}{R_0 \sinh^2 \rho_0}. \tag{5.7}$$

It is noted that for a fixed R_0, the curvature $\kappa_{\max}$ increases as ρ_0 decreases and actually one has that $\kappa_{\max} \to \infty$ as $\rho_0 \to +0$. In what follows, we shall also need the conormal derivative of a function $\psi(x)$ defined over ∂D. Let ∂D be parametrized as $x(s)$, and then the conormal derivative of $\psi(x)$ is defined as

$$\mathrm{d}\psi = \psi'(x) \cdot \frac{x'(s)}{|x'(s)|} = \frac{\mathrm{d}}{\mathrm{d}s}\psi(x(s))\frac{1}{|x'(s)|}.$$

Proposition 5.3. *Let ∂D be an ellipse described in (5.2) and (5.4), and let $\phi_{1,n}$ and $\phi_{2,n}$ be the NP eigenfunctions derived in Lemma 5.2 for $K^*_{\partial D}$ with $n \geq 1$. Then one has*

(1) $\phi_{1,n}(x)$ achieves its maximum absolute value on ∂D at $x_\circ$ and x_*,

$$|\phi_{1,n}(x_\circ)| = |\phi_{1,n}(x_*)| = \tau_{\max}, \quad \tau_{\max} := \frac{1}{R \sinh \rho_0}, \tag{5.8}$$

and there holds the following asymptotic relationship as $\kappa_{\max} \to +\infty$, or equivalently $\rho_0 \to +0$,

$$\tau_{\max} \sim \alpha \kappa_{\max}^p, \quad p = 1/2, \quad \alpha \in \mathbb{R}_+. \tag{5.9}$$

(2) $d\phi_{2,n}$ achieves its maximum absolutely value on ∂D at $x_\circ$ and x_*,

$$|d\phi_{2,n}(x_\circ)| = |d\phi_{2,n}(x_*)| = \tau'_{\max}, \quad \tau'_{\max} := \frac{n}{R_0 \sinh^2 \rho_0}, \tag{5.10}$$

and moreover there holds

$$\tau'_{\max} \to \infty \quad \text{as} \quad \kappa_{\max} \to \infty. \tag{5.11}$$

(3) $S_{\partial D}[\phi_{1,n}]$ and $dS_{\partial D}[\phi_{2,n}]$, respectively, achieve their maximum absolute values at $x_\circ$ and x_*.

Proof. With the explicit forms of solutions in Lemma 5.2, the proposition can be verified by straightforward though a bit tedious calculations. □

In Proposition 5.3, we did not consider the case with $n = 0$ due to Lemma 5.1. Clearly, the properties in Proposition 5.3 can be used to explain the localization and geometrization phenomenon discovered in Section 4, at least for the elliptic geometry case. In fact, we perform the numerical experiment in Figure 3 again, but with the plasmonic inclusion ∂D in Figure 2 replaced by an ellipse in Figure 4. The loss parameter δ is set to be 0.0001. The total wave field is plotted in Figure 5. Clearly, strong resonant behaviours are observed locally around the two high-curvature points $x_\circ$ and x_*. It is remarked that the incident plane wave propagates from the left to the right and the vertex $x_\circ$ is located in the shadow region. Hence, the resonant behaviour around x_* is stronger than that around $x_\circ$.

We believe those beautiful geometric structures in Proposition 5.3 for the NP eigenfunctions and the associated single-layer potentials hold for more general geometries. However, dealing with the general geometries, it is unpractical to derive the explicit forms of the NP eigenfunctions and the associated single-layer potentials. We have conducted extensive numerical experiments within general geometries and indeed the NP eigenfunctions exhibit certain intrinsic geometric structures near a boundary point with a high curvature. Before presenting our discoveries, we first introduce the notion of a symmetric domain. Consider a star-shaped domain D whose boundary ∂D is parametrized as follows,

$$\partial D = r(\theta)\hat{x}(\theta), \quad \hat{x}(\theta) = (\cos\theta, \sin\theta), \quad \theta \in [0, 2\pi), \tag{5.12}$$

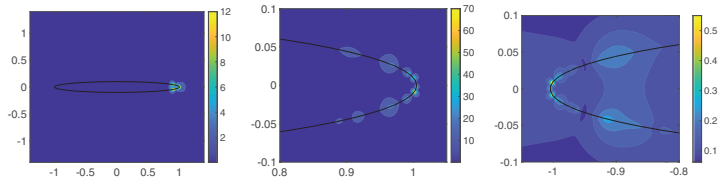

(a) (b) (c)

FIGURE 5. Localization and geometrization phenomenon in the plasmon resonance associated with an elliptical inclusion. (a) Modulus of the total wave field around the whole plamsonic inclusion; (b), (c) Modulus of the total wave field around x_* and x_o, respectively.

where $r \geq 0$ is a smooth radial function. If there exists $n \in \mathbb{N}$ such that

$$r(\theta) = r(\theta + 2\pi/n), \tag{5.13}$$

the the domain D is said to be n-symmetric. Clearly, the domain in Figure 2 is 1-symmetric and the domain in Figure 4 is 2-symmetric. An n-symmetric domain possesses n high-curvature points.

The major numerical discoveries can be summarized as follows:

(1) Suppose D is convex with ∂D satisfying (5.12), and $\lambda \in \sigma(K^*_{\partial D})$. If λ is positive and simple, then the absolute values of both its eigenfunction and the corresponding single-layer potential blow up at the high-curvature point(s) on ∂D as the corresponding curvature goest to infinity; whereas if λ is positive and multiple, then there exists at least one of the eigenfunctions such that the absolute values of both the eigenfunction and the associated single-layer potential blow up at the high-curvature point(s) on ∂D as the corresponding curvature goest to infinity. If λ is negative, then similar conclusions hold at the high-curvature point(s), but for the conormal derivatives of the eigenfunction and the associated single-layer potential.
(2) Suppose D is concave at the high-curvature point(s) with ∂D satisfying (5.12), and $\lambda \in \sigma(K^*_{\partial D})$. If λ is negative and simple, then the absolute values of both its eigenfunction and the associated single-layer potential blow up at the high-curvature point(s) on ∂D as the corresponding curvature goest to infinity; whereas if λ is positive and multiple, then there exists at one of the eigenfunctions such that the absolute values of both the eigenfunction and the associated single-layer potential blow up at the high-curvature point(s) on ∂D as the corresponding curvature goest to infinity. If λ is positive, then similar conclusions hold at the high-curvature point(s), but for the conormal derivatives of the eigenfunction and the associated single-layer potential.
(3) If D is non-symmetric, then the NP eigenfunction or its conormal derivative as well as the corresponding single-layer potential may still possess the blow-up behaviour at a high-curvature point, but the situation is more complicated, and there is no definite conclusion about it.

As mentioned earlier, we have conducted extensive numerical experiments to support the above assertions. In what follows, we only present a few representative ones and we also refer to the arXiv preprint version of this paper [18] for more numerical examples.

5.1. Numerical method

We first introduce the numerical method used to calculate the spectral system of the NP operator defined in (2.10) and the corresponding single layer potential. Assume that the boundary of D, i.e. ∂D, is parameterized by $r(t)$, $t \in (0, 2\pi)$. Then the NP operator can be expressed as follows

$$K^*[\varphi](x) = \frac{1}{2\pi} \int_0^{2\pi} \frac{\langle r(s) - r(t), \nu_s \rangle}{|r(s) - r(t)|^2} \varphi(r(t)) |r'(t)| \mathrm{d}t. \tag{5.14}$$

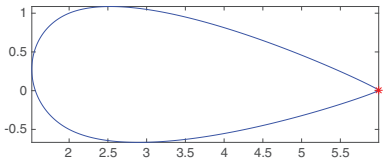

FIGURE 6. A convex 1-symmetric domain.

To numerically calculate this integral, we first discretize the integral line into n panels and on each panel, we utilize the 16-point Gauss-Legendre quadrature formula. We point out that from the expression in (5.14), there is the singularity when $t = s$, namely $y = x$. However, noting that $r(t) \in C^2(\partial D)$, the singularity can be removed by using the following identity,

$$\lim_{t\to s} \frac{\langle r(s) - r(t), \nu_s\rangle}{|r(s) - r(t)|^2} = -\frac{\langle r''(s), \nu_s\rangle}{2|r'(s)|^2},$$

where ν_s signifies the exterior unit normal vector to ∂D at $r(s)$.

5.2. A convex 1-symmetric domain

Let us first consider a domain D with one high-curvature point, denoted as x_*, as shown in Figure 6, and the largest curvature is 500. The first seven largest NP eigenvalues (in terms of the absolute value) are numerically found to be

$$\begin{gathered}\lambda_0 = 0.5, \quad \lambda_1 = 0.2575, \quad \lambda_2 = -0.2575, \quad \lambda_3 = 0.1365,\\ \lambda_4 = -0.1365, \quad \lambda_5 = 0.0685, \quad \lambda_6 = -0.0685.\end{gathered} \tag{5.15}$$

It is remarked that all of the eigenvalues are simple.

Figure 7 plots the eigenfunctions as well as the associated single-layer potentials, respectively, for the positive eigenvalues $\lambda_1 = 0.2575$ and $\lambda_3 = 0.1365$. The numerical results clearly support our assertion about the NP eigenfunctions associated to simple positive eigenvalues.

Figure 8 plots the eigenfunctions as well as the corresponding conormal derivatives and single-layer potentials for the negative eigenvalues $\lambda_2 = -0.2575$ and $\lambda_4 = -0.1365$, respectively. The numerical results clearly support our assertion about the NP eigenfunctions associated to simple negative eigenvalues.

We also numerically investigate the blow-up rate of the eigenfunction or its conormal derivative at a high-curvature point and find that they always follow the following rule

$$\psi_{\max} \sim a\kappa_{\max}^p \quad \text{as} \quad \kappa_{\max} \to +\infty, \tag{5.16}$$

where $\alpha, p \in \mathbb{R}_+$ and $\psi_{\max}$ signifies the absolute value at the high-curvature point for the eigenfunction if the corresponding eigenvalue is positive, and for the conormal derivative of the eigenfunction if the eigenvalue is negative. In fact, by increasing the curvature at the point x_* and using a standard regression, we can find the blow-up rates for different eigenvalues in (5.15). The parameters from the regression are listed in Table 1.

5.3. A convex 3-symmetric domain

In this subsection, we consider a convex 3-symmetric domain as shown in Figure 9, which possesses three high-curvature points that are denoted by x_*, $x_\triangle$ and x_o as shown in Figure 9. The largest curvature is

$$\kappa_{x_*} = \kappa_{x_\triangle} = \kappa_{x_o} = 500. \tag{5.17}$$

The first seven largest eigenvalues (in terms of the absolute value) are numerically found to be

$$\lambda_0 = 0.5, \ \lambda_1 = \lambda_2 = 0.2850, \ \lambda_3 = \lambda_4 = -0.2850, \ \lambda_5 = 0.2583, \ \lambda_6 = -0.2583. \tag{5.18}$$

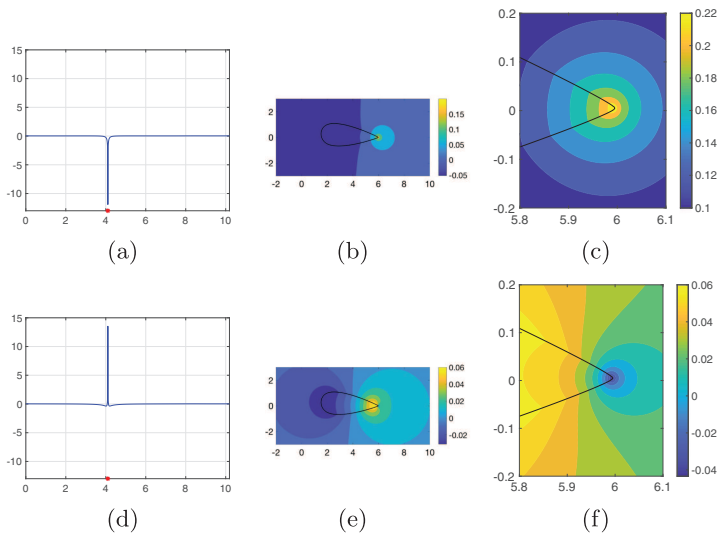

FIGURE 7. (a) Plotting of the eigenfunction for $\lambda_1 = 0.2575$ with respect to the arc length; (b) The associated single-layer potential for $\lambda_1 = 0.2575$; (c) The single-layer potential around the high-curvature point; (d–f) The corresponding items for $\lambda_3 = 0.1365$.

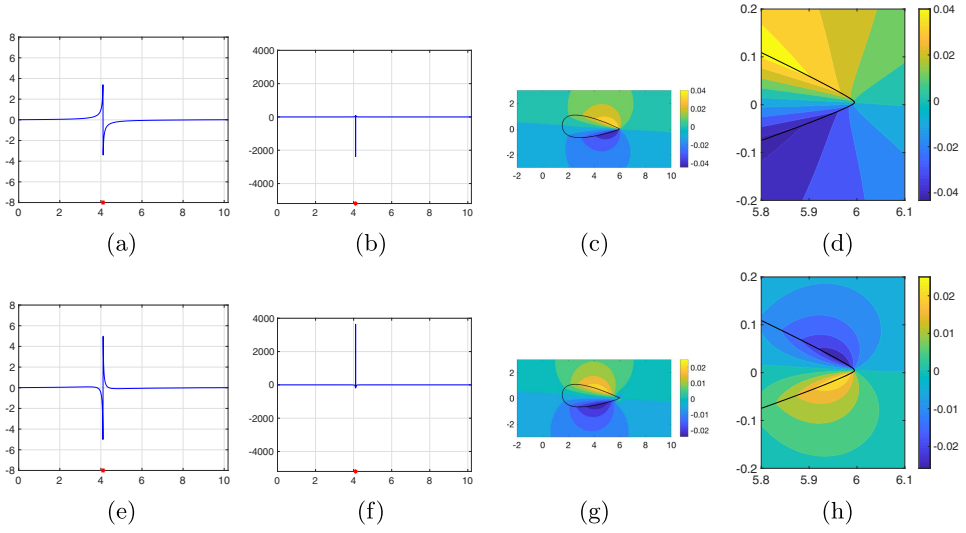

FIGURE 8. (a), (b) Plotting of the eigenfunction and its conormal derivative for $\lambda_2 = -0.2575$; (c), (d) The associated single-layer potential for $\lambda_2 = -0.2575$; (e–g) The corresponding items for the negative eigenvalues $\lambda_4 = -0.1365$.

Compared to the study in the previous subsection, there are multiple NP eigenvalues occurring for the 3-symmetric domain. Hence, we can verify our assertion about the NP eigenfunction associated to a multiple NP eigenvalue. Nevertheless, for those simple eigenvalues, one can draw completely same conclusions about their eigenfunctions as those discovered in the previous subsection; see the arXiv preprint version of the paper [18] for the numerical results. For illustration, we only present the numerical results associated with the eigenvalues λ_1 and λ_2.

TABLE 1. The parameters of the form (5.16) from the regression associated with the eigenvalues in (5.15): (a) $\lambda_j, j = 1, 3, 5$; (b) $\lambda_j, j = 2, 4, 6$.

(a)

	λ_1	λ_3	λ_5
p	0.4793	0.4824	0.4925
$\ln(\alpha)$	−0.5022	−0.3886	−0.3867

(b)

	λ_2	λ_4	λ_6
p	1.4108	1.3602	1.3423
$\ln(\alpha)$	−1.0102	−0.2763	−0.1483

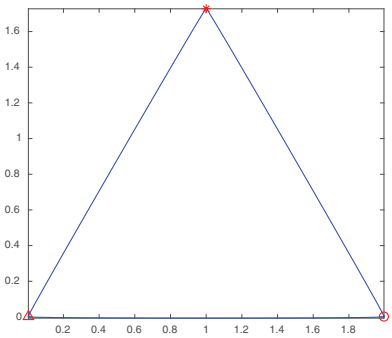

FIGURE 9. A convex 3-symmetric domain.

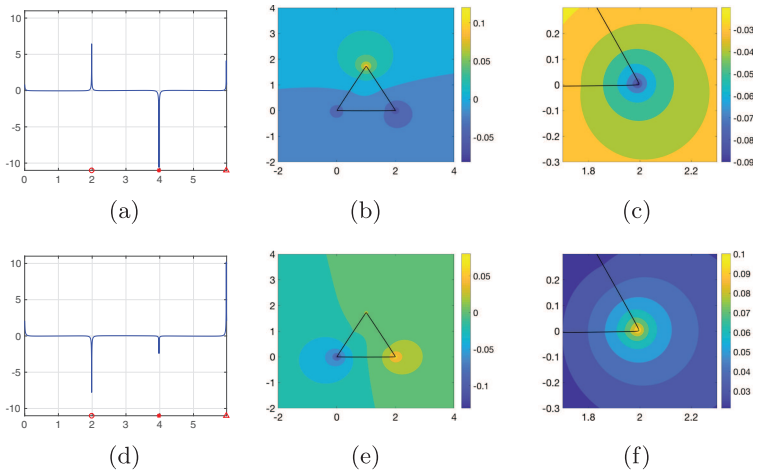

FIGURE 10. (a–c) The first eigenfunction associated with $\lambda_1 = \lambda_2 = 0.2850$ as well as the corresponding single-layer potential; (d–f) The second eigenfunction associated with $\lambda_1 = \lambda_2 = 0.2850$ as well as the corresponding single-layer potential.

Figure 10 plots the two linearly independent eigenfunctions associated with the multiple eigenvalue $\lambda_1 = \lambda_2 = 0.2850$, as well as the corresponding single-layer potentials. The numerical results clearly support our assertion about the NP eigenfunctions associated with multiple NP eigenvalues. We refer to [18] again for the case with $\lambda_3 = \lambda_4 = -0.2850$, and the numerical results also support our earlier assertion.

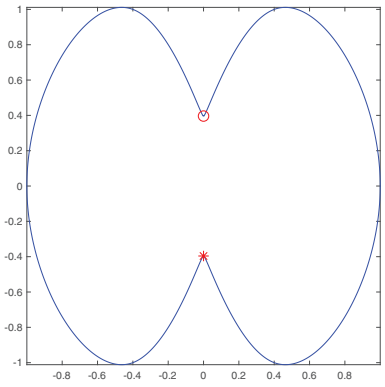

FIGURE 11. A concave 2-symmetric domain.

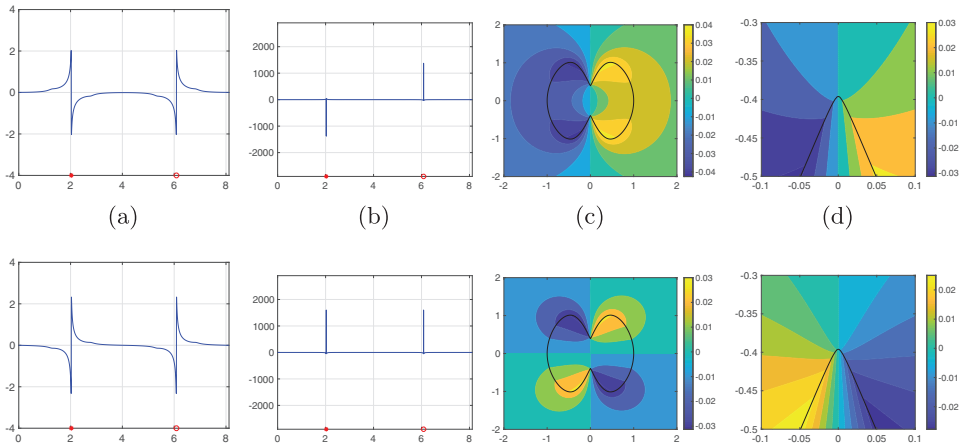

FIGURE 12. (a–d) The eigenfunction, its conormal derivative, and the corresponding single-layer potential associated with $\lambda_1 = 0.3676$; (e–h) The corresponding items associated with $\lambda_3 = 0.3303$.

5.4. A concave 2-symmetric domain

In this subsection, we consider a concave 2-symmetric domain as shown in Figure 11, which possesses two high-curvature points that are denoted by x_* and x_o. The largest curvature is

$$\kappa_{\max} = \kappa_{x_*} = \kappa_{x_o} = 500. \tag{5.19}$$

The first five largest NP eigenvalues (in terms of the absolute value) are

$$\begin{gathered} \lambda_0 = 0.5, \quad \lambda_1 = 0.3676, \quad \lambda_2 = -0.3676, \quad \lambda_3 = 0.3303, \\ \lambda_4 = -0.3303, \quad \lambda_5 = 0.2347 \quad \lambda_6 = -0.2347. \end{gathered} \tag{5.20}$$

Figure 12 plots the eigenfunctions, their conormal derivatives and the associated single-layer potentials, respectively, associated with the eigenvalues $\lambda_1 = 0.3676$ and $\lambda_3 = 0.3303$. The numerical results clearly support our earlier assertion about the NP eigenfunctions associated with simple positive eigenvalues.

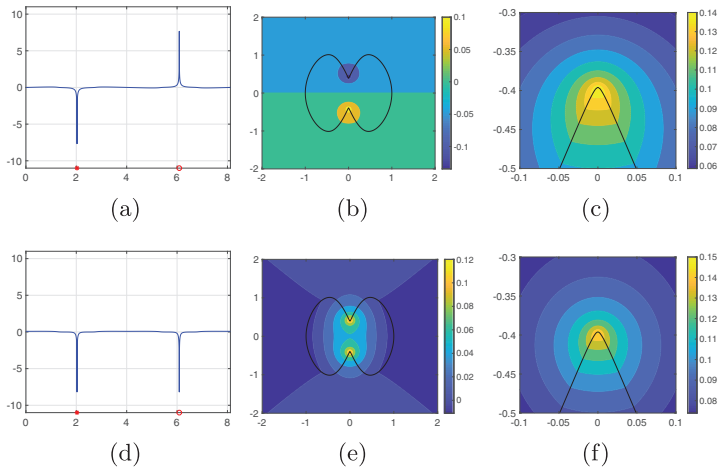

FIGURE 13. (a–d) The eigenfunction, its conormal derivative, and the corresponding single-layer potential associated with $\lambda_2 = -0.3676$; (e–h) The corresponding items associated with $\lambda_4 = -0.3303$.

TABLE 2. The parameters of the form (5.16) from the regression associated with the eigenvalues in (5.20): (a) $\lambda_j, j = 1, 3, 5$; (b) $\lambda_j, j = 2, 4, 6$.

(a)

	λ_1	λ_3	λ_5
p	1.4415	1.4604	1.3742
$\ln(\alpha)$	−1.7389	−1.7075	−0.6801

(b)

	λ_2	λ_4	λ_6
p	0.4836	0.4963	0.4729
$\ln(\alpha)$	−0.9712	−0.9860	−0.6875

Figure 13 plots the eigenfunctions, their conormal derivatives and the associated single-layer potentials, respectively, associated with the eigenvalues $\lambda_2 = -0.3676$ and $\lambda_4 = -0.3303$. The numerical results clearly support our earlier assertion about the NP eigenfunctions associated with simple negative eigenvalues.

We next investigate the blow-up rate of the NP eigenfunction or its conormal derivative with respect to the curvature. It turns out that blow-up rate also follows the rule in (5.16). By regression, we numerically determine the corresponding parameters for those different eigenvalues in (5.20), and they are listed in Table 2.

5.5. A non-symmetric domain

In this subsection, we consider a non-symmetric domain as shown in Figure 14, which possesses three boundary points with relatively large curvatures that are marked as x_o, x_* and $x_\triangle$ in the figure. The corresponding curvatures at those three points are respectively given as

$$\kappa_{x_o} = 500, \quad \kappa_{x_*} = \kappa_{x_\triangle} = 41. \tag{5.21}$$

It is noted that the domain in Figure 14 is different from the one in Figure 9. Here, we modify the curvatures at the two points x_* and $x_\triangle$ such that the domain is no longer symmetric. Obviously, x_o is the high-curvature point.

First, the first five largest NP eigenvalues (in terms of the absolute value) associated with ∂D in Figure 14 are numerically found to be

$$\lambda_0 = 0.5, \quad \lambda_1 = 0.2710, \quad \lambda_2 = -0.2710, \quad \lambda_3 = 0.2320, \quad \lambda_4 = -0.2320. \tag{5.22}$$

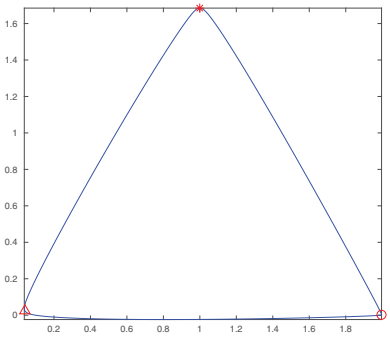

FIGURE 14. A non-symmetric domain.

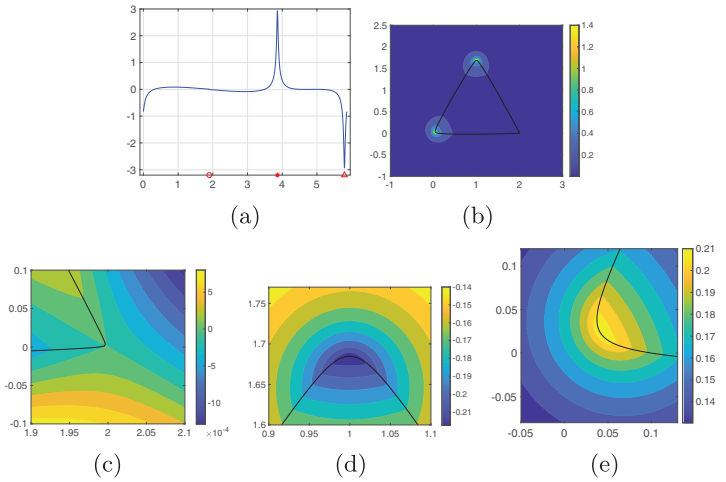

FIGURE 15. (a) Eigenfunction with respect to the arc length associated to the eigenvalue $\lambda_3 = 0.2320$; (b) The corresponding single-layer potential; (c–e) The single-layer potential around the three points x_o, x_* and $x_\triangle$, respectively.

Figure 15 plots the eigenfunction and the corresponding single-layer potential around the three points x_o, x_* and $x_\triangle$ associated to the eigenvalue $\lambda_3 = 0.2320$. It can be readily seen that the blow-up behaviour does not occur at the high-curvature point x_o, and instead it occurs at the two points x_* and $x_\triangle$ which possesses relatively large curvatures.

Figure 16 plots the eigenfunction, and its conormal derivative as well as the corresponding single-layer potential associated to the eigenvalue $\lambda_4 = -0.2320$. It can be readily seen that the blow-up behaviour of the conormal derivative does not occur at the high-curvature point x_o, and instead it occurs at the two points x_* and $x_\triangle$ again.

Clearly, the previous two examples show that the blow-up behaviour does not follow the one observed for symmetric domains. The two points x_* and $x_\triangle$ are symmetric with respect to x_o, and they two may compete with the point x_o to form the blow-up behaviours as observed above. However, there are no definite rules for this and in [18], one more non-symmetric example can be found.

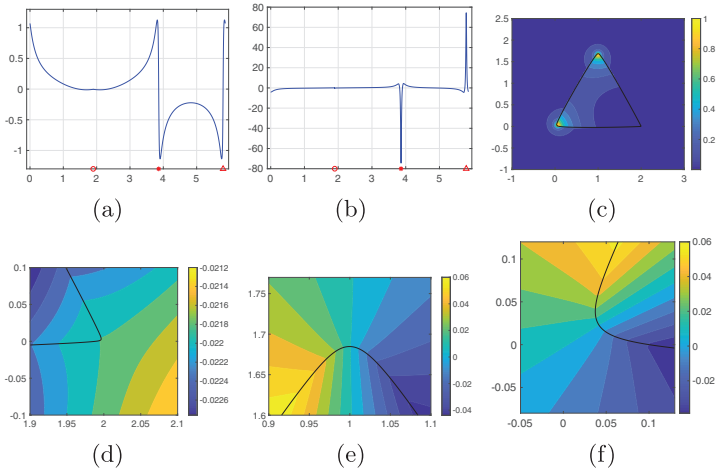

FIGURE 16. (a), (b) Eigenfunction and its conormal derivative with respect to the arc length associated to the eigenvalue $\lambda_4 = -0.2320$; (c–f) The corresponding single-layer potential as well as their behaviours around the three points x_o, x_* and $x_\triangle$, respectively.

6. Concluding remarks

In this paper, we showed that the Neumann-Poincaré eigenfunctions possess certain delicate and intriguing geometric structures. The results are of independent interest and significant importance in the spectral theory for the Neumann-Poincaré operator. Furthermore, the results can be used to explain the localization and geometrization phenomanon in the plasmon resonances, which is another interesting discovery made in the present article. The localization and geometrization phenomena might be used to produce super-resolution effect in wave imaging. To illustrate this, we present a last numerical example. Consider a plasmonic inclusion D as plotted in Figure 17, whose parametrization is given by

$$r(\theta) = 1 + 0.0001e^{8\sin(12\theta)}. \tag{6.1}$$

There are 12 cusped points and we denote that by $r_{\max}\hat{x}_n$, $n = 0, 1, \ldots, 11$, where

$$r_{\max} = 1 + 0.0001e^{8}, \quad \hat{x}_n = \hat{x}(\pi/24 + n\pi/6), \quad n = 0, 1, \ldots, 11.$$

It is easily seen that the distance $\tilde{d}$ between two cusped points is

$$\tilde{d} = |r(\max)\hat{x}_n - r(\max)\hat{x}_{n+1}| = 0.6719. \tag{6.2}$$

Now, let us choose the plasmon parameters inside the domain D as follows,

$$\epsilon_c = -2.48907 \quad \text{and} \quad \delta = 0.00001,$$

which follows the rule in (2.13), since one of the NP eigenvalues of the operator $K^*_{\partial D}$ can be numerically determined to be

$$\lambda = 0.21339.$$

We also take an incident plane wave of the form (3.14) with the wave number k replaced by $k = 0.01$. By our earlier discussion on the localization and geometrization in plasmon resonances, it can be observed that strong resonant behaviours occur around the cusped points which possess very large curvatures. Those resonant

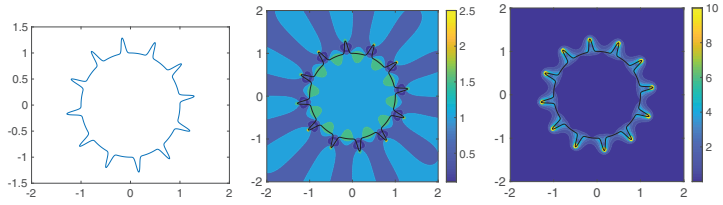

(a) (b) (c)

FIGURE 17. *Left*: A star-shaped plasmonic inclusion. *Middle*: Modulus of the resonant field. Right: Modulus of the gradient of the field.

behaviours can apparently be used to locate those cusp parts on the plasmonic inclusion. However, we note that the underlying wavelength is given by

$$\lambda = 2\pi/k = 628.32,$$

which is much bigger than $\tilde{d}$ in (6.2). Hence, one might expect to have a certain super-resolution imaging effect. In this last example, we also note that $k \cdot \mathrm{diam}(D) \approx 0.02$, which means that the localization and geometrization phenomenon occurs at an even finer scale in the quasi-static regime. Clearly, this is mainly due to the peculiar geometric structures of the NP eigenfunctions near high-curvature points. As emphasized earlier, we mainly relied on extensive numerical experiments and considered the two-dimensional case in our study. It is worth of further investigation on the three-dimensional case as well as the corresponding theoretical justifications.

Acknowledgements. The work of H. Liu was supported by the Hong Kong RGC GRF grants (projects 12302017, 12301218 and 12302919). The authors would like to thank the two anonymous referees for their constructive comments and suggestions that led to significant improvements on the presentation and results of the paper.

REFERENCES

[1] H. Ammari, G. Ciraolo, H. Kang, H. Lee and G.W. Milton, Spectral theory of a Neumann–Poincaré-type operator and analysis of cloaking due to anomalous localized resonance. *Arch. Ration. Mech. Anal.* **208** (2013) 667–692.

[2] H. Ammari, G. Ciraolo, H. Kang, H. Lee and G.W. Milton, Spectral theory of a Neumann–Poincaré-type operator and analysis of cloaking due to anomalous localized resonance II. *Contemp. Math.* **615** (2014) 1–14.

[3] H. Ammari, Y. Deng and P. Millien, Surface plasmon resonance of nanoparticles and applications in imaging. *Arch. Ration. Mech. Anal.* **220** (2016) 109–153.

[4] H. Ammari, B. Fitzpatrick, H. Kang, M. Ruiz, S. Yu and H. Zhang, Mathematical and computational methods in photonics and phononics, In Vol. 235 of *Mathematical Surveys and Monographs*. American Mathematical Society, Providence, RI (2018).

[5] H. Ammari, P. Millien, M. Ruiz and H. Zhang, Mathematical analysis of plasmonic nanoparticles: The scalar case. *Arch. Ration. Mech. Anal.* **224** (2017) 597–658.

[6] H. Ammari, M. Ruiz, S. Yu and H. Zhang, Mathematical analysis of plasmonic resonances for nanoparticles: The full Maxwell equations. *J. Differ. Equ.* **261** (2016) 3615–3669.

[7] K. Ando, Y. Ji, H. Kang, K. Kim and S. Yu, Spectral properties of the Neumann–Poincaré operator and cloaking by anomalous localized resonance for the elastostatic system. *Eur. J. Appl. Math.* **29** (2018) 189–225.

[8] K. Ando, Y. Ji, H. Kang, K. Kim and S. Yu, Cloaking by anomalous localized resonance for linear elasticity on a coated structure. *SIAM J. Math. Anal.* **49** (2017) 4232–4250.

[9] K. Ando, H. Kang and H. Liu, Plasmon resonance with finite frequencies: A validation of the quasi-static approximation for diametrically small inclusions. *SIAM J. Appl. Math.* **76** (2016) 731–749.

[10] K. Ando, H. Kang and Y. Miyanishi, Elastic Neumann–Poincaré operators on three dimensional smooth domains: Polynomial compactness and spectral structure. *Int. Math. Res. Not.* **2019** (2019) 3883–3900.

[11] K. Ando, H. Kang and Y. Miyanishi, Spectral structure of elastic Neumann–Poincaré operators. *J. Phys.: Conf. Ser.* **965** (2018) 012027

[12] E. Blåsten and H. Liu, Scattering by curvatures, radiationless sources, transmission eigenfunctions and inverse scattering problems. Preprint: arXiv:1808.01425 (2018).

[13] G. Bouchitté and B. Schweizer, Cloaking of small objects by anomalous localized resonance. *Q. J. Mech. Appl. Math.* **63** (2010) 438–463.

[14] O.P. Bruno and S. Lintner, Superlens-cloaking of small dielectric bodies in the quasistatic regime. *J. Appl. Phys.* **102** (2007) 124502.
[15] D. Chung, H. Kang, K. Kim and H. Lee, Cloaking due to anomalous localized resonance in plasmonic structures of confocal ellipses. *SIAM J. Appl. Math.* **74** (2014) 1691–1707.
[16] Y. Deng, H. Li and H. Liu, On spectral properties of Neumann–Poincaré operator and plasmonic resonances in 3D elastostatics. *J. Spectr. Theory* **9** (2019) 767–789.
[17] Y. Deng, H. Li and H. Liu, Analysis of surface polariton resonance for nanoparticles in elastic system. Preprint: arXiv:1804.05480 (2018).
[18] E. Blåsten, H. Li, H. Liu and Y. Wang, Localization and geometrization in plasmon resonances and geometric structures of Neumann–Poincaré eigenfunctions. Preprint: arXiv:1809.08533 (2018).
[19] J. Helsing, H. Kang and M. Lim, Classification of spectra of the Neumann–Poincaré operator on planar domains with corners by resonance. *Ann. Inst. Henri. Poincaré-AN* **34** (2017) 991–1011.
[20] Y. Ji and H. Kang, A concavity condition for existence of a negative Neumann–Poincaré eigenvalue in three dimensions. Preprint: arXiv:1808.10621 (2018).
[21] H. Kang and D. Kawagoe, Surface Riesz transforms and spectral property of elastic Neumann–Poincaré operators on less smooth domains in three dimensions. Preprint: arXiv:1806.02026 (2018).
[22] H. Kang, M. Lim and S. Yu, Spectral resolution of the Neumann–Poincaré operator on intersecting disks and analysis of plasmon resonance. *Arch. Ration. Mech. Anal.* **226** (2017) 83–115.
[23] H. Kettunen, M. Lassas and P. Ola, On absence and existence of the anomalous localized resonace without the quasi-static approximation, *SIAM J. Appl. Math.* **78** (2018) 609–628.
[24] D.M. Kochmann and G.W. Milton, Rigorous bounds on the effective moduli of composites and inhomogeneous bodies with negative-stiffness phases. *J. Mech. Phys. Solids* **71** (2014) 46–63.
[25] R.V. Kohn, J. Lu, B. Schweizer and M.I. Weinstein, A variational perspective on cloaking by anomalous localized resonance. *Comm. Math. Phys.* **328** (2014) 1–27.
[26] R.S. Lakes, T. Lee, A. Bersie and Y. Wang, Extreme damping in composite materials with negative-stiffness inclusions. *Nature* **410** (2001) 565–567.
[27] H. Li and H. Liu, On anomalous localized resonance for the elastostatic system. *SIAM J. Math. Anal.* **48** (2016) 3322–3344.
[28] H. Li and H. Liu, On three-dimensional plasmon resonance in elastostatics. *Annali di Matematica Pura ed Applicata* **196** (2017) 1113–1135.
[29] H. Li and H. Liu, On anomalous localized resonance and plasmonic cloaking beyond the quasistatic limit. *Proc. R. Soc. A* **474** 20180165.
[30] H. Li, J. Li and H. Liu, On quasi-static cloaking due to anomalous localized resonance in $\mathbb{R}^3$. *SIAM J. Appl. Math.* **75** (2015) 1245–1260.
[31] H. Li, J. Li and H. Liu, On novel elastic structures inducing plariton resonances with finite frequencies and cloaking due to anomalous localized resonance. *J. Math. Pures Appl.* **120** (2018) 195–219.
[32] H. Li, S. Li, H. Liu and X. Wang, Analysis of electromagnetic scattering from plasmonic inclusions beyond the quasi-static approximation and applications. *ESAIM: M2AN* **53** (2019) 1351–1371.
[33] R.C. McPhedran, N.-A.P. Nicorovici, L.C. Botten and G.W. Milton, Cloaking by plasmonic resonance among systems of particles: Cooperation or combat? *C. R. Phys.* **10** (2009) 391–399.
[34] D.A.B. Miller, On perfect cloaking. *Opt. Exp.* **14** (2006) 12457–12466.
[35] G.W. Milton and N.-A.P. Nicorovici, On the cloaking effects associated with anomalous localized resonance. *Proc. R. Soc. A* **462** (2006) 3027–3059.
[36] G.W. Milton, N.-A.P. Nicorovici, R.C. McPhedran, K. Cherednichenko and Z. Jacob, Solutions in folded geometries, and associated cloaking due to anomalous resonance. *New J. Phys.* **10** (2008) 115021.
[37] J.C. Nédélec, Acoustic and electromagnetic equations, In Vol. 144 of *Applied Mathematical Sciences*. Springer-Verlag, New York (2001).
[38] N.-A.P. Nicorovici, R.C. McPhedran, S. Enoch and G. Tayeb, Finite wavelength cloaking by plasmonic resonance. *New J. Phys.* **10** (2008) 115020.
[39] N.-A.P. Nicorovici, R.C. McPhedran and G.W. Milton, Optical and dielectric properties of partially resonant composites. *Phys. Rev. B* **49** (1994) 8479–8482.
[40] N.-A.P. Nicorovici, G.W. Milton, R.C. McPhedran and L.C. Botten, Quasistatic cloaking of two-dimensional polarizable discrete systems by anomalous resonance. *Opt. Exp.* **15** (2007) 6314–6323.
[41] G.W. Milton and N.-A.P. Nicorovici, On the cloaking effects associated with anomalous localized resonance. *Proc. R. Soc. A* **462** (2006) 3027–3059.
[42] J.B. Pendry, Negative refraction makes a perfect lens. *Phys. Rev. Lett.* **85** (2000) 3966.
[43] D.R. Smith, J.B. Pendry and M.C.K. Wiltshire, Metamaterials and negative refractive index. *Science* **305** (2004) 788–792.
[44] V.G. Veselago, The electrodynamics of substances with simultaneously negative values of ϵ and μ. *Sov. Phys. Usp.* **10** (1968) 509–514.